

Article

A Feature Engineering-Assisted CM Technology for SMPS Output Aluminium Electrolytic Capacitors (AEC) Considering D-ESR-Q-Z Parameters

Akeem Bayo Kareem  and Jang-Wook Hur *

Department of Mechanical Engineering (Department of Aeronautics, Mechanical and Electronic Convergence Engineering), Kumoh National Institute of Technology, 61 Daehak-ro, Gumi-si 39177, Gyeongsang-buk-do, Korea; akeembayo79@yahoo.com

* Correspondence: hhjw88@kumoh.ac.kr

Abstract: Recent research has seen an interest in the condition monitoring (CM) approach for aluminium electrolytic capacitors (AEC), which are present in switched-mode power supplies and other power electronics equipment. From various literature reviews conducted and from a failure mode effect analysis (FMEA) standpoint, the most critical and prone to fault component with the highest percentage is mostly capacitors. Due to its long-lasting ability (endurance), CM offers a better paradigm for AEC due to its application. However, owing to severe conditions (over-voltage, mechanical stress, high temperature) that could occur during use, they (capacitors) could be exposed to early breakdown and overall shutdown of the SMPS. This study considered accelerated life testing (electrical stress and long-term frequency testing) for the component due to its endurance in thousands of hours. We have set up the experiment test bench to monitor the critical electrical parameters: dissipation factor (D), equivalent series resistance (ESR), quality factor (Q), and impedance (Z), which would serve as a health indicator (HI) for the evaluation of the AECs. Time-domain features were extracted from the measured data, and the best features were selected using the correlation-based technique.

Keywords: aluminum electrolytic capacitor; condition monitoring; fault diagnosis; feature engineering; LCR meter; switched mode power supply



Citation: Kareem, A.B.; Hur, J.-W. A Feature Engineering-Assisted CM Technology for SMPS Output Aluminum Electrolytic Capacitors Considering D-ESR-Q-Z Parameters. *Processes* **2022**, *10*, 1091. <https://doi.org/10.3390/pr10061091>

Academic Editors: Mohand Djeziri and Marc Bendahan

Received: 10 May 2022

Accepted: 26 May 2022

Published: 30 May 2022

Publisher's Note: MDPI stays neutral with regard to jurisdictional claims in published maps and institutional affiliations.



Copyright: © 2022 by the authors. Licensee MDPI, Basel, Switzerland. This article is an open access article distributed under the terms and conditions of the Creative Commons Attribution (CC BY) license (<https://creativecommons.org/licenses/by/4.0/>).

1. Introduction

Indeed, it is necessary to ensure that the design of components and systems used in practical applications achieves an optimal percentage level of efficiency, durability, and reliability. The core concept of prognostics and health management (PHM) is to avoid unforeseen breakdowns and economic loss. PHM plays a progressively important role in modern power electronics device condition-based maintenance (PED-CBM). It helps to estimate the health conditions of a particular component in the system. However, some factors can diminish the reliability, and durability of a system, such as environmental conditions, which would go a long way in either causing timely failure or sudden shutdown of the systems [1–5]. Recent studies/research have changed the dynamics and approach to maintenance, which involves the integration of diagnosis, fault detection and identification (FDI), and prognosis, and can be termed “conditioned-based maintenance” (CBM), unlike traditional-based maintenance (preventive maintenance). Owing to the scarcity of data, most researchers work mainly with the model-based [6–9] approach, which requires empirical and analytical models compared to the data-driven approach [10–13]. In power converters, the most vulnerable components are capacitors and switching devices. The pictorial view of the electrolytic capacitor is shown in Figure 1a. Figure 1b shows the various fault-prone components in power electronic devices, and Figure 1c shows the stress distribution, and the root cause of failure in power converters [14,15].

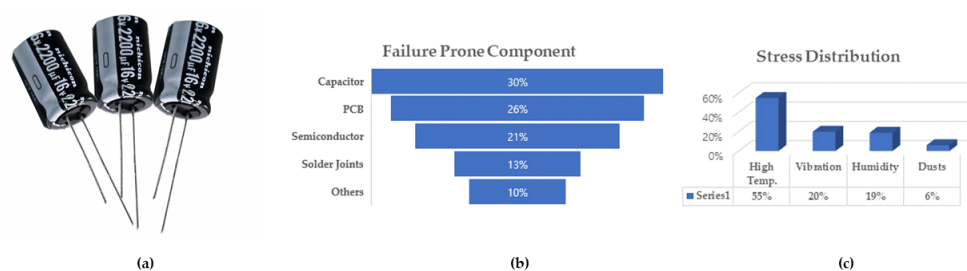


Figure 1. A representation of the fault prone components in power electronic systems, (a) A typical 16 V 1000 uf aluminum electrolytic capacitor (b) Root cause breakdown and (c) Common causes of failure in power electronics.

When developing a predictive model using machine learning or statistical modelling, “feature engineering” refers to leveraging domain expertise to choose and convert the most critical variables from raw data. Feature engineering and selection aim to make machine learning (ML) algorithms perform better. The model you choose, the data you have, and the features you prepare all influence the outcomes you get. Even the way you frame the problem and the objective measurements you use to determine correctness have an impact. Several interconnected factors influence your outcomes. Significant characteristics that describe the structures of your data are required [13,16–18].

When building speedier and smaller electrical gadgets, high-performance components are essential. The capacitor is an excellent example, as it is frequently used to achieve meagre equivalent series resistance (ESR). This attribute means that capacitors with this property have a high-quality factor Q , or, in other words, minimal loss or dissipation D . The capacitor’s ESR, or equivalent series resistance, as well as its DF, or dissipation factor, loss tangent, and Q , or quality factor, are all critical aspects in its specification. Many elements of a capacitor’s operation, including the ESR, dissipation factor, loss tangent, and Q , are significant. They can determine the applications for which the capacitor can be utilized. ESR, DF, and Q are all elements of a capacitor’s performance that impact its durability and efficiency. However, for capacitors used in power supplies, ESR and DF are essential since a high ESR and dissipation factor, DF, will result in a considerable quantity of power being dissipated in the capacitor [14,19,20].

The concept of accelerated life testing has been widely geared for application in capacitors owing to the time it takes for them to degrade under several conditions. The concept was utilized in the aging, with experimental investigation showing that an escape of electrolytes from the capacitor would result in a decrease in the capacitance value and an increase in the ESR value. Also, several papers have addressed the fault diagnosis of capacitors using offline techniques [21–23].

The genuine interest of this research is to achieve a condition monitoring approach that captures the key failure-prone component—capacitors (but not limited to)—found in SMPS. In this study, we will be making the following contributions:

- A multi-parameter-based health condition monitoring approach covers the equivalent series resistance, impedance, loss factor, and quality factor. These selected electrical parameters have shown a better paradigm for the degradation of electrolytic capacitors.
- A more robust data acquisition technique involving the HIOKI 3536 industry standard for wide application is aided by a software application to control and set the required measurement conditions for each capacitor.
- A robust feature engineering approach using a statistical time-domain feature extraction approach for each capacitor data-set (D , R_s , Q , Z) and a correlation-based feature selection. This approach has helped select the best features and reduction process and not forget the critical concept of data preprocessing techniques that require data wrangling, reshaping, normalization, and cleaning.

- A machine learning-based algorithm set was selected to train and test the new data set. Due to the nature of the data size and how the data were acquired, the befitting models for these were the ML-classifier models.

The structure of this paper is arranged as follows: Section 2 covers the motivation, literature review, and related works. In contrast, Section 3 gives reviews of the various theories used in the study. Section 4 shows the proposed framework for the condition monitoring of the aluminium electrolytic capacitor, while Section 5 shows the experimental setup for data collection. Section 6 discussed the experimental results and the selected knowledge-based classification algorithms. Section 7 describes the conclusion and future work.

2. Motivation, Literature and Related Works

From various FMEAs conducted on SMPS, the most fault-prone component is the output capacitors, saddled with the function of withstanding high-frequency voltage ripples and keeping a steady output voltage of 12 V, 5 V, and 3.3 V for their various applications. The increasing evaporation of the electrolyte is the leading cause of degradation in most AEC, which increases the value of equivalent series resistance (ESR) and decreases the value of the capacitance (C) concerning the time of usage. Degradation can either lead to power loss, unstable output voltage, or shutdown of the entire system (SMPS) [23].

The condition monitoring and diagnostics of capacitors can be classified into an online and an offline process, with the latter having been neglected in the past years. However, the offline process, which involves the detachment of the capacitors from the SMPS, is less expensive, easier to use, and causes no damage to the overall SMPS system. On the one hand, there is an established theory that once the ESR value of a capacitor doubles, i.e., twice its initial value, it is regarded that the life of the capacitors in question has ended. On the other hand, there is established knowledge of other electrical parameters like capacitance, impedance showing degradation trends and acting as a health indicator tool for diagnostics. The measurement of ESR, one of the major health indicators for electrolytic capacitors, can be achieved using an LCR. However, the accuracy in the data acquisition prompts an improvement in a more high-precision instrument.

A diagnostics process involving the injection of a controlled ac component into a three-phase AC/DC converters, which can be classified as an online technique owing to the methodology, is carried out in [24]. The value of the ESR can be computed by manipulating these ac voltages and current components with digital filters, with the recursive least squares technique providing reliable estimation results. Furthermore, the ESR value is rectified by considering the temperature effect, for which a simple temperature-sensing circuit was constructed. ESR is a decision-making tool for the three-phase AC/DC PWM converters. Interestingly, another approach involving the use of magnetic sensors was used to estimate the ESR using capacitor and inductor current [25]. The process was proven to have improved the accuracy of the ESR prediction in AEC found in boost converters. However, another methodology involving the use of short-time Fourier transform (STFT) was proposed in [26], which involves the use of the C and ESR parameters. The only need for the proposed method is the acquisition of the capacitor voltage and current signals and a boost converter used in several simulated and experimental tests. Based on the various electrical parameters that can serve as a health indicator tool, the dissipation factor acted as a diagnostic tool for DC-link capacitors in [27]. It is possible to estimate the switching component of the capacitor current by measuring the power converter's output currents rather than measuring the capacitor current using this technique. The proposed approach is simulated, and the effects of several aspects on the accuracy of the dissipation factor measurement were explored. This and many recent approaches can be classified as online techniques using simulations. While they must have achieved some accuracy with their various proposed technique, which is as a result of utilizing the output voltage or current of the power converters to estimate the degradation and condition monitoring of the capacitors [28–33]. The efficiency of this approach lacks any practical in-depth as to an experimental approach hence the need for a condition monitoring approach using

an offline method and comparing the results with an online approach—as done in [34,35]. The aforementioned study also proved that there is no developed approach to achieve a condition monitoring for electrolytic capacitor applicable in SMPS while in use except by designing a typical setup similar to the SMPS or other applicable devices. Hence, in this study, we have deployed a more efficient approach that utilizes the integration of feature engineering advantages and the decision-making avenue, i.e., selecting the suitable model based on a combination of features.

3. Theoretical Backgrounds

3.1. Working Description for AEC in SMPS

In generality, the working framework of the SMPS is to utilize the switching devices (IGBT, MOSFET) to convert an unregulated voltage from the input capacitor (mainly at a higher voltage range) to a regulated and smoothed DC output voltage (12 volts, 5 volts and 3.3 volts). There are numerous criteria to consider in selecting the input and output filters due to the design and reliability process, namely, equivalent series resistance, rated ripple current, and rated voltage. The input capacitors receive current at a higher range repeatedly compared to the output capacitors that receive smoothed output ripple voltage—this is assisted by the presence of the inductor in series with the output capacitor, which then serves as an output filter. Interestingly, the SMPS efficiency is based on the following standpoints:

- The S in SMPS stands for switching, which denotes varying voltage continuously.
- The output voltage is controlled by the switching time effect, which is dependent on the feedback circuitry
- The design efficiency is high because instead of releasing the excess power from the SMPS as heat, it tends to continuously regulate the input (using the switching device) to control the output

Due to the above-listed advantages, the SMPS is applicable in motherboards of computers, mobile phone chargers, high voltage direct current (HVDC) power transmission measurements, battery chargers, central power distribution, motor vehicles, and consumer electronics, laptops, security systems, space stations.

3.2. Degradation Mechanism of an Aluminum Electrolytic Capacitors

A high capacitance yet small-sized capacitor is created with the increased effective surface area obtained by etching the foil and achieved by interlacing two strips of aluminium foil (anode and cathode) with paper. This foil and paper are then wound into an element and electrolyte embedded. AEC will degrade performance and eventually fail when exposed to high voltages. In practice, however, the liquid electrolyte, electrolytic capacitor plates, and aluminium oxide can all cause a modest equivalent series resistance (ESR). AEC are constantly subjected to a high voltage/electrical over-stress to accelerate their degradation to acquire the capacitance value and ESR in an acceptable amount of time. The electrolytic capacitor charges and discharges continually, deteriorating with time as the electrolyte evaporates, the leakage current increases, and the internal pressure rises [36].

The current in the AEC surges when a DC voltage is given to a discharged electrolytic capacitor. During the charge and discharge cycle, the current flow raises the electrolytic capacitor's internal temperature. The electrolyte will progressively evaporate as the temperature rises. As a result, the ESR rises while the capacitance decreases. The oxide layer can deteriorate due to the periodic temperature cycle caused by the charge and discharge of the electrolytic capacitor. Despite an insulating layer between the two plates, a tiny leakage current will develop in the electrolytic capacitor, and the leakage current will increase as the oxide layer degrades. The ESR and capacitance value will be influenced when the leakage current increases. The increase in pressure inside the electrolytic capacitor is another degradation avenue because that contributes to its degeneration. The gas inside the electrolytic capacitor is formed by the rising internal temperature and the increased pace of the chemical reaction during the charging/discharging cycle. The growing gas can raise the electrolytic capacitor's internal pressure [37–41].

3.3. Overview of Machine Learning-Based Algorithms

In general, a classification model is a function that weights the input features so that the output separates one class into positive and negative values, respectively. The weights (and functions) that offer the most accurate and best separation of the two groups of data are identified during the training of the classifier models. To identify the performance of a classifier, one must subject them to some metrics like f1 score, accuracy, sensitivity/recall, and precision. The equations for these metrics are properly defined in Equations (7)–(10) with various applications in some related works [42]. The decision tree model will create classification rules based on the properties of the training dataset and the classes supplied. The selection of the “optimal split parameter” for the prediction decision is the decision tree’s fundamental restriction. This issue can be addressed by using a random forest classifier, a combination of ensemble and decision tree classification. It is a combination of a bagging approach and a decision tree-based method. Random forest generates several decision trees for accurate and steady prediction and combines them. The random forest classifier has several advantages, including solving classification and regression problems, which makes it a popular choice in today’s machine learning systems. It describes the optimized model by examining the most important attributes from a randomly generated subset of features [43–46]. Stochastic gradient descent (SGD) is a simple yet effective method for learning discriminative linear classifiers with convex loss functions, such as (linear) support vector machines and logistic regression. Because it updates more often, SGD can converge quicker on big datasets than batch training [47–49].

Support vector classifier (SVC) has the merit of solving small sample and nonlinear problems quickly, and there is no local minimum problem. SVC is also capable of dealing with high-dimensional data sets and has good generalization skills. On the other hand, SVC struggles to explain the high-dimensional mapping of kernel functions, notably radial basis functions. When the data has been confirmed, it is vulnerable to substantial variances and missing data. The relevance to problems involving many classifications is limited. The pace of the Naive Bayes model is rapid for classifier problems. It has many advantages when processing actual data samples, and it offers incremental operations that can train fresh samples. However, using the assumption of sample attribute independence is NB’s fatal flaw. The classification performance will rapidly deteriorate when the sample properties are correlated. A logistic function is used in the logistic regression (LR) model to represent the probability of an outcome occurring. This method is the most useful when you want to know how numerous independent variables affect a single result variable. The most popular feed-forward neural network is the multi-layer perceptron (MLP). MLP comprises three levels: an input layer, an output layer, and the hidden layers in between. The hidden layer in MLP provides the computation and processing capacity that allows the network output to be generated. The loss function of an MLP with hidden layers is non-convex, and there are several local minimums. As a result, various random weight initialization can result in varying validation accuracy. To reduce all errors, the gradient boost model will continue to improve. This can lead to over-fitting by exaggerating outliers. Cross-validation is used to resolve the above problem attributed to the MLP model [50]. Computationally expensive—GB frequently necessitates many trees (>1000), which can take a long time and consume much memory. During tuning, this necessitates a massive grid search [51,52]. Adaboost is less prone to overfitting because the input parameters are not all tuned simultaneously. Adaboost can help weak classifiers increase their accuracy. Rather than binary classification challenges, Adaboost is now utilized to categorize text and images. Adaboost’s key disadvantage is that it requires a high-quality dataset. Before using an Adaboost algorithm, avoid using noisy data and outliers [53,54]. In a supervised situation, when we are provided with a dataset with target labels, k nearest neighbours (KNN) can be utilized for classification. KNN selects the k closest data points in the training set for classification, and the target label is computed as the mode of the target label of these k nearest neighbours. When used for classification and regression, it can learn nonlinear decision boundaries. It can devise a highly adaptable decision boundary by

varying the value of k. The value of k is the only hyper-parameter and helps to facilitate hyperparameter adjustment [55–58].

4. Proposed Integrated Feature Engineering and ML-Based Methods

The proposed architecture for the condition monitoring framework is shown in Figure 2. The filter-based feature selection has been introduced using a data-driven approach to enhance and improve the discriminating features between the capacitors selected. Interestingly, the model consists of the pre-processing data stage, a 3-way feature extraction, correlation-based feature selection, a different combination of input variables, ML-based diagnosis and performance evaluation of the selected ML algorithm. The dataset comprising the ESR, Z, Q, and D was subsequently received by the model for statistical feature extraction for each set of capacitors with their description shown in Table 1. The dataset acquisition occurs using the software aided platform and the LCR meter. The LCR meter has an inbuilt capacity to obtain four electrical parameters during the data acquisition process. The other electrical parameters achievable with the LCR meter are as follows: Admittance (Y), Impedance phase angle, Conductance (G), Susceptance (S), Inductance (Ls and Lp), Capacitance (Cp and Cs), DC resistance (Rdc), Conductivity, Permittivity, and Reactance (X).

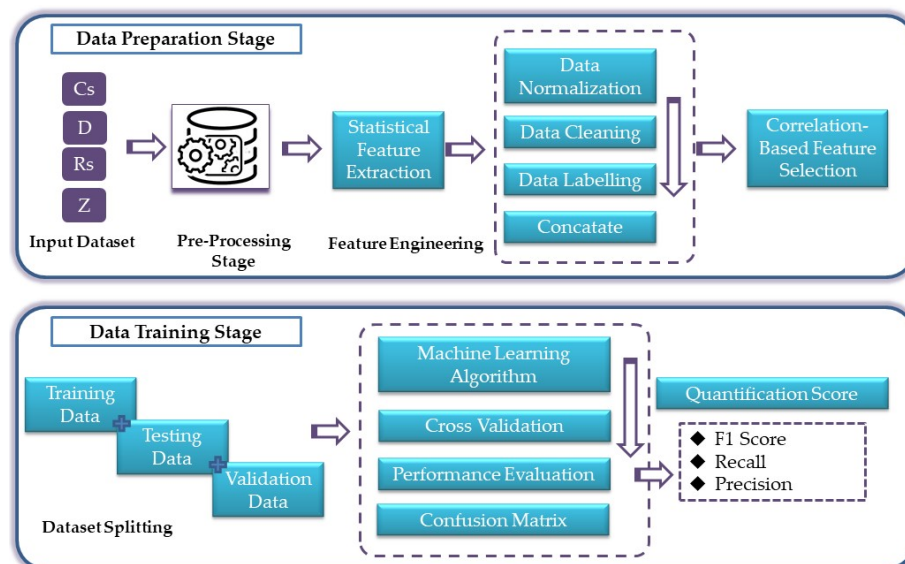


Figure 2. The proposed condition monitoring framework for the SMPS Aluminum Electrolytic Capacitors.

Table 1. The Feature Set Description.

Parameters	Definition	Functions
Z	Impedance	$Z = \frac{ X_c }{\sin\theta}$
D	Loss coefficient/Dissipation Factor	$\tan\delta = \frac{ESR}{X_c}$
Rs	Equivalent Series Resistance	$ESR = Z \cos\theta$
Q	Quality Factor	$Q = \frac{X_c}{ESR}$

The basic idea of feature selection is subjective to removing non-informative or redundant predictors from the model. Interestingly, the performance of a machine learning model could degrade if input parameters that are not relevant to the target variable are given. In order to decide on which methods of feature selection to be deployed, it is best to ascertain if the outcome is supervised or unsupervised. The time domain features summarized in Table 2 were extracted using a reshaping technique to transform the structure of the dataset row and column format. As shown in Figure 3, it can be observed in red colour that there

are highly correlated features such as variance, root mean square, mean, and maximum value out of the 21 features extracted. In comparison, seven features were selected after using the correlation techniques in Equation (1) namely mean, interquartile range, kurtosis, fifth quartile, wave factor, minimum value, and median absolute deviation. The features selected, as shown in Figure 4 were chosen based on a correlation benchmark of 0.7. The features extraction and selection vary accordingly based on the input variables, either showing more or less discriminative features and showing more or more minor features selected [42,59].

$$\rho_{X,Y} = \frac{\text{cov}(X, Y)}{\sigma_X \sigma_Y} \tag{1}$$

where σ_X and σ_Y are the standard deviations of X and Y , respectively while $\text{cov}(X, Y)$ is the covariance.

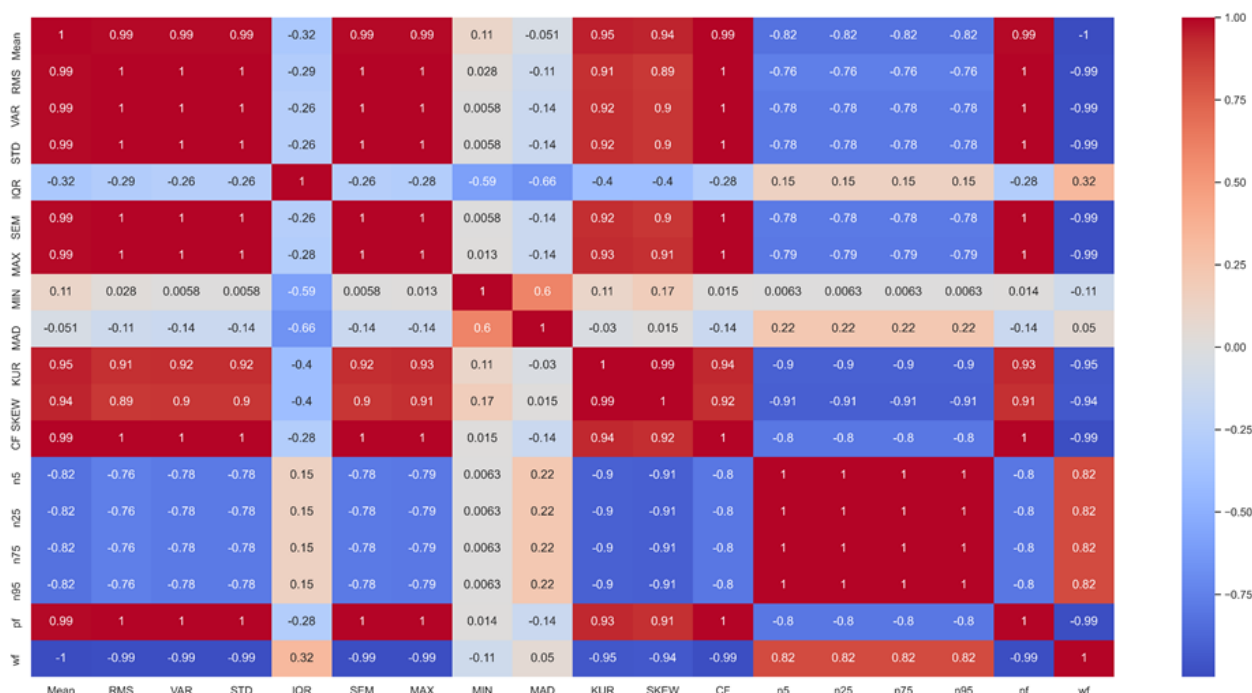


Figure 3. Correlation Matrix for all the features extracted.



Figure 4. Correlation Matrix for the features selected.

Table 2. Statistical Extracted Features and their definitions [42].

Feature Name	Definition
n th percentile ($n = 5, 25, 75, 95$)	$P_x = 100 \frac{x-0.5}{n}$
Root Mean Square	$X_{rms} = \sqrt{\frac{\sum_{i=1}^n (x_i)^2}{n}}$
Mean	$\bar{x} = \frac{1}{n} (\sum_{i=1}^n x_i)$
Kurtosis	$X_{kurt} = \frac{1}{N} \sum \left(\frac{(x_i - \mu)^3}{\sigma} \right)$
Interquartile range	upperquarter Q_3 – lowerquarter Q_1
Median abs deviation	$X_{mad} = \frac{1}{n} \sum_{i=1}^n x_i - m $
Skewness	$X_{skew} = E \left[\left(\frac{(x_i - \mu)^3}{\sigma} \right) \right]$
Max	$X_{max} = \max(x_i)$
Min	$X_{min} = \min(x_i)$
Crest Factor	$X_{CF} = \frac{x_{max}}{x_{rms}}$
Peak factor	$x_{PF} = \frac{x_{max}}{\sqrt{x_s}}$
Wave Factor	$x_{WF} = \frac{\sqrt{\frac{1}{n} \sum_{i=1}^n x_i ^2}}{\frac{1}{n} \sum_{i=1}^n x_i }$
Standard error mean	$X_{sem} = \frac{\text{standard deviation}}{\sqrt{n}}$
Standard deviation	$SD = \sqrt{\frac{1}{N-1} \sum_{i=1}^N (x_i - \bar{x})^2}$
Variance	$VAR = \sqrt{\frac{1}{N} \sum_{i=1}^N (x_i - \bar{x})^2}$

5. Data Acquisition Process

The proposed CM technology for acquiring multiple electrical parameters was achieved using the HIOKI 3536 LCR meter (IM3536) with an high-precision measurement of $\pm 0.05\%$ rdg and high-speed measurement of 1 ms. The IM3536 offers a wide function range of DC and frequency from 4 MHz to 8 MHz, which has raised the industry standard for a general-purpose LCR meter. The three standalone capacitors applicable in the SMPS were used as the case study for the CM technology. An LCR meter and CV (constant-voltage) mode can measure voltage dependency samples. The CV was selected when changes in the input voltage were not required at both ends of the test sample. Compared to the V mode, the CV model has the potential to run the experiment continuously when the voltage value is monitored and controlled with feedback. Firstly, calibration is recommended for the equipment before usage. The open and short correction process was carried out prior to the commencement of the experiment. The residual components in the test fixture used to measure a target can be stated using the equivalent circuit. Both of these correcting methods are “open and short corrections”, and LCR meters have the functionality to conduct both. The instrument is set to match the frequency of the power source to reduce the noise effect. To avoid unstable measurement, the supply frequency matches the commercial power frequency (50/60 Hz) [60,61]. The data acquisition process is better described in Figure 5 showing the computer-aided software, HIOKI 3536 LCR meter, the L2000 four-terminal probe connected to the end of the LCR meter holds the test sample as shown in Figure 5. The data collection process lasted 4320 min at room temperature for all capacitors starting with the highest capacity—2200 uf, 1000 uf and 470 uf. The experimental condition is best described in Table 3. The impedance Z has a real section (R_s) and an imaginary (X) section, and its parameters can be determined by expanding it on a complex plane. The impedance relationships are expressed in the Equations (2)–(6) below:

$$Z = R_s + jX = |Z|\angle\theta \quad (2)$$

$$\theta = \tan^{-1}\left(\frac{X}{R_s}\right) \quad (3)$$

$$R_s = |Z|\cos\theta \quad (4)$$

$$X = |Z|\sin\theta \quad (5)$$

$$|Z| = \sqrt{R_s^2 + X^2} \quad (6)$$

Table 3. Experimental Measurement Conditions.

Functions	Description
Electrical Parameters	D-Rs-Q-Z
Frequency/Freq-Step	1 MHz/1000 Hz/10 Hz
DC Bias	ON 1.0 volts
Signal Level	0.5 Vrms
Measurement Range	Auto
Speed	SLOW2
LowZ mode	ON

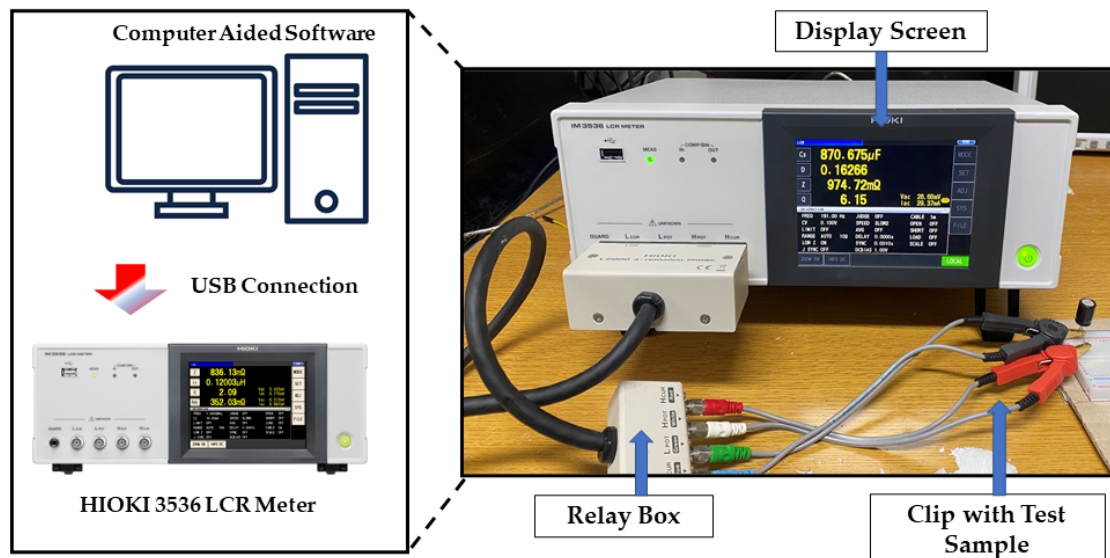


Figure 5. A detailed description of the connection used in data acquisition process.

5.1. Experimental Test Bench

The capacitors were subjected to 4 Hz to 8 MHz using computer-aided software to provide the necessary parameters for a frequency-based mode. The description for the computer-aided software process of data acquisition is shown in Figures 6–8. The equipment with the device under test (DUT) was subjected to the following:

1. USB Communication Selection—This window showcase the selection process for the correct USB port for the connection between the computer, software and the equipment. Once there is no synchronization between the System, the equipment will not proceed with the data collection process.
2. System—Setting up the equipment system covers the measurement type 1–4 with the necessary parameters. The level mode has the option for constant voltage (CV),

- constant current (CC) and open-circuit voltage (V). The latter was selected during the experimental procedure to achieve a varying voltage across the DUT. The AC speed was selected for the SLOW2 option to provide the slowest and high accuracy for the DUT parameters selected. The Low Z mode on the dashboard provides a high precision when set ON for capacitors with high capacitance above 100 μf . The Ac auto range is kept On to provide an automatic range for the DUT. The Limit (A) is set off to not interfere with the current generated during the DUT test procedure.
- Fix Function—The set of frequency (Hz), DC Bias (V), and AC level (V) are set to fix the value. The sampling delay function is needed to enter the delay needed during measurement. However, for capacitor measurement, we do not need this function. The sampling mode function consists of the infinite mode (na), finite (Ea) and Timer(sec). The infinite mode was selected during the experiment to achieve a continuous measurement until the frequency set is reached.
 - DC Sweep—These functions consist of the DC bias start voltage, DS-Frequency (Hz), Dc Bias Stop (v), DS-AC level (V), DC Bias Step Voltage, and DS-Delay (sec). The start and stop voltage were set to 1 volt and 5 volts, respectively, while the step voltage was set to 0.01 volts which means there would be an increase during the measurement in the order 0.01, 0.02, 0.03 till the set stop voltage.
 - Frequency Sweep—This covers the frequency start, stop and step, which were set to 10, 8 MHz and ten, respectively.
 - Operation Start and Stop—This section covers the reset, setup, run, stop, and the close button, which aids the measurement parameter settings and program end button.
 - Graph Buffer Size—From this section, you can easily manoeuvre between the two graph windows and view the run and stop the display. Also, select the preferred parameter (Y-axis) for each graph and the x-axis section, which could be frequency, and the number of samples.
 - Measured Data—This section displays in rows and columns the measured data from the DUT.
 - Measured Data Plot—This section plots the graph for the first two selected parameters with both on the y axis (left and right) with a common x-axis.
 - Graph Setting—This section gives room for adjustment and controls to the graph section, which could help in quick visualization while the experiment is ongoing.

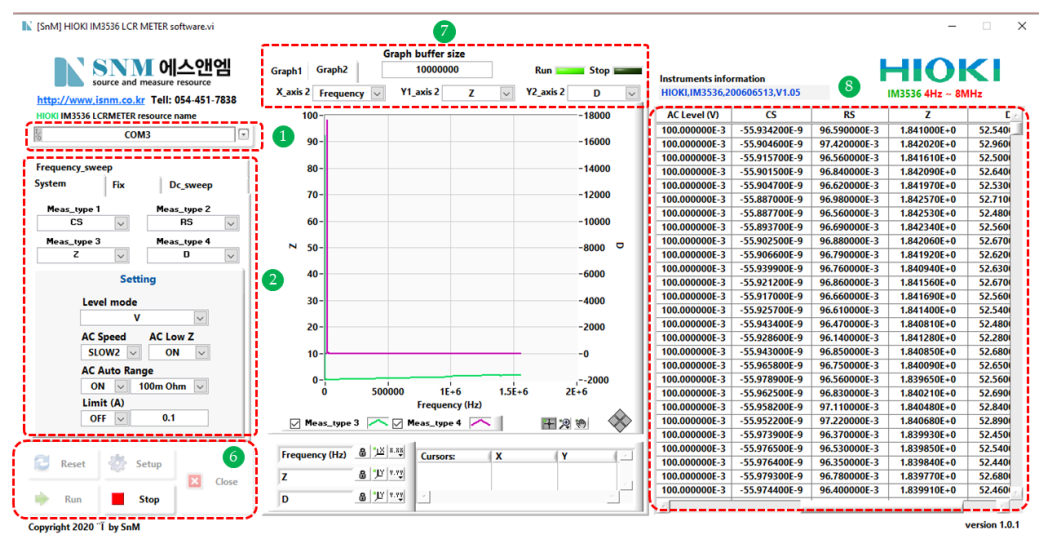


Figure 6. A detailed description of the computer aided software interface used in data collection with label from 1, 2, 6, 7 and 8.

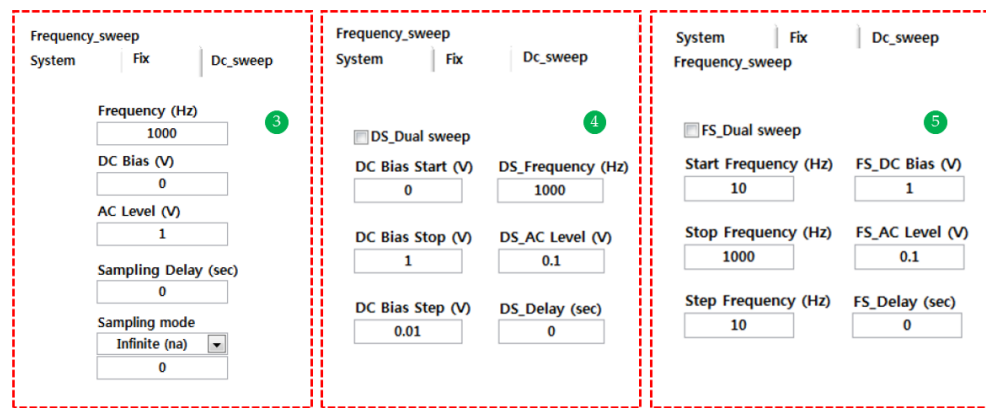


Figure 7. A description of the section numbered 3 to 5 covering the Fix function, DC-Sweep and Frequency Sweep respectively.

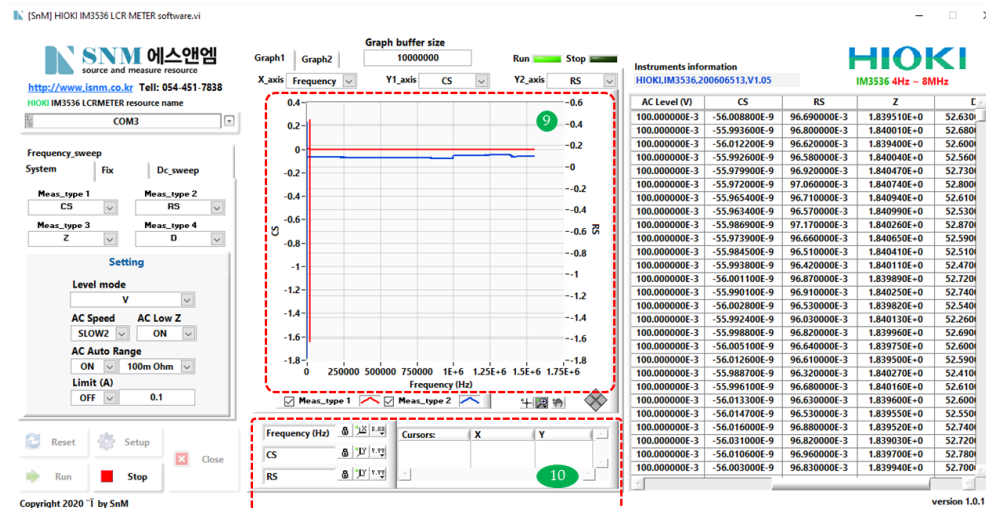


Figure 8. A further description for the computer aided section of 9 and 10 showing the graph display and graph setting/adjustment section.

Equivalent Circuit Mode and LCR Meter Measurement Circuit—The Four Terminal Pair Method

By detecting the current flowing to the measurement target and the voltage across the measurement target’s terminals, LCR meters can determine Z and phase angle. They then use the Z and phase angle values to calculate measurement parameters like inductance (L), capacitance (C), and resistance (R). Whether the instrument is in series equivalent circuit mode or parallel equivalent circuit mode, the equations utilized to calculate these measurement parameters change as the instrument cannot decide which mode is appropriate for a given measurement objective. The user must select the proper equivalent circuit mode to minimize measurement error. Figure 9 shows the description of the four terminal pair measurement circuit used for the data acquisition process [62,63].

Cs (or Ls) and the resistance component Rs are linked in series in series equivalent circuit mode, whereas Cp (or Lp) and the resistance portion Rp are connected in parallel equivalent circuit mode. In general, series equivalent circuit mode is used when measuring low-impedance elements (with an impedance of fewer than 100 ohms), such as high-capacity capacitors and low inductance. The parallel equivalent circuit mode is used when measuring high-impedance elements (with an impedance of more than 10 k ohms), such as low-capacitance capacitors and high-inductance. Both data sets can be displayed since measured values in both equivalent circuit modes are calculated values. However, caution is advised since the optimal equivalent circuit depends on the measurement aim.

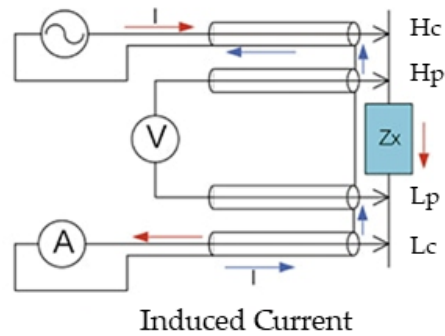


Figure 9. The LCR meter measurement circuit—Four Terminal Pair Method.

By decreasing the impacts of the magnetic field induced by the measurement current, this approach can reduce measurement error from impedance values ranging from low to high. By employing insulated cables and overlaying the cables conveying current to and from the measurement target, it can neutralize the magnetic field.

5.2. Experimental Data Visualization

Following the experiment carried out using the HIOKI 3536 LCR meter, the results of the ESR are shown in Figure 10. For a better comparison, the experiment also involved other electrical parameters like dissipation factor (D), impedance (Z), and quality factor (Q) for three electrolytic capacitors applicable as an output filter for SMPS. The capacitors measured have a nominal capacitance value of 2200 uf, 1000 uf, 470 uf and 16 volts across the capacitors, respectively. It can be seen from Figure 10 that there is a degradation trend among the capacitors as they are subjected to a charging and discharging cycle but at a minimal voltage value of 1.0 to 5.0 volts.

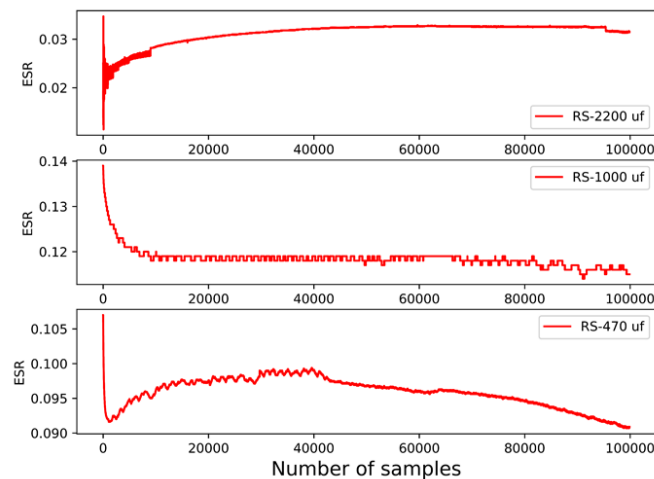


Figure 10. Exploratory time series data analysis of the equivalent series resistance (ESR) across the three capacitors.

6. Diagnostics Assessment and Discussion

6.1. Selected Algorithm Parameters

There are huge interrelationships between extracted condition health indicators/features as most machine learning classifiers would require discriminant characteristics as input to achieve acceptable diagnostic accuracy. Figure 4 shows the feature selection results, which should offer sufficient and acceptable diagnostic results and act as the correct condition indicators for aluminium electrolytic capacitors used in SMPS. The 7-dimensional selected

features are extracted from the training and test data sets, respectively, and prepared for ML-based diagnosis training and evaluations. However, there is an increase and reduction based on the input variables picked when the idea of combining and eliminating different input features to be extracted is used. We have considered the selected ML-based classifiers due to prior knowledge, robustness, and computational costs. The selected algorithms are shown in Table 4. Each model has its own set of parameters and design, necessitating domain knowledge for optimal performance. The machine learning algorithms are implemented based on the python programming language using a system with the following configurations; processor (AMD Ryzen 7 2700 Eight Core Processor, 3.20 GHz), installed memory (32 GB RAM), system type (64-bit operating system, x64-based processor).

Table 4. Machine Learning Classifiers and their Parameters.

ML Classifier	Major Functional Parameters	Parameter Values
MLP	Activation function (f), number of layers/nodes (h/a), learning rate (α)	$2^*f = \text{ReLU}, h/a = 1/7, \alpha = 0.001$
DT	max-depth	3
KNN	k	3
RF	n estimators	70
SGD	random-state	101
NB	loss function = modified huber	–
LR	Gaussian, var-smoothing = $1e-09$	–
GBC	Regularization	L1, L2
SVC	n estimators	100
Adaboost	Regularization (C), gamma (γ)	$C = 100, \gamma = \text{auto}$
	n estimators	50

6.2. Machine Learning Assessment Evaluation

The accuracy of a classification algorithm is an important factor to consider when evaluating its performance. The accuracy of a classification method on a data set is defined as the number of instances predicted correctly over the total number of instances when all instances in the data set have the same weight. K-fold cross-validation is a popular method for predicting the performance of a classification algorithm or comparing the performance of two classification algorithms on a data set. This approach divides a data set into k disjoint folds of roughly similar size at random, with each fold being used to test the model induced by the other $k-1$ folds via a classification algorithm. The average of the k accuracy obtained from k -fold cross-validation is used to evaluate the classification algorithm's performance, and the level of average is considered to be at fold [64,65]. These classification metrics formula—accuracy, recall/sensitivity, precision, and f1 score are shown in Equations (7)–(10). In addition, the confusion matrix provides a more in-depth analysis of the performance of the selected algorithms on the dataset.

$$\text{Accuracy} = \frac{TP}{TP + FP + TN + FN} \quad (7)$$

$$\text{Recall/Sensitivity} = \frac{TP}{TP + FN} \quad (8)$$

$$\text{Precision} = \frac{TP}{TP + FP} \quad (9)$$

$$\text{F1-Score} = \frac{2 * \text{Sensitivity} * \text{Precision}}{\text{Precision} + \text{sensitivity}} \quad (10)$$

where the true positives (TP) are the number of correctly classified predictions, and true negatives (TN) are the number of classified that are negative and are negative. False positives (FP) are the number of falsely classified predictions that are positive, and the false

negatives (FN) are the number of incorrectly labelled inputs belonging to an incorrectly classified class. The model with the least FN is best chosen as it is the best criteria for implementation and choosing the suitable model [42].

Table 5 summarises the performance comparison among the ML models selected based on all the electrical parameters acting as an input variable to the models. As observed from Table 5, the RDF and GB have a 99.77% and 100 % accuracy with a computational cost (s) of 17.5067 and 55.4777, respectively. However, KNN and SVC show a 99.33% and 94.33% accuracy with a lesser computational cost of 0.3133 and 1.0400, respectively. RDF and GB seem to have a higher rank than KNN and SVC in terms of accuracy. However, from the standpoint of cost, the KNN and SVC can be categorized as the best model for selection using all the features, i.e., the four electrical parameters selected during the experimental setup. The NB with the least computational cost of 0.2667 shows a poor prediction accuracy of 34.55%, making it rank the least and not to be considered for deployment. Figure 11 shows the plot of all the models in terms of accuracy (in green colour) and computational cost (in black dashed line).

Table 5. Global performance comparison of ML models using all feature sets.

Algorithm	Accuracy (%)	Precision (%)	Recall (%)	F1-Score (%)	Cost (s)
MLP	58.89	48.17	57.33	49.49	8.2444
DT	91.11	93.28	92.00	91.81	0.4467
KNN	99.33	98.68	98.67	98.67	0.3133
RDF	99.77	96.13	95.78	95.77	17.5067
SGD	73.88	67.90	70.11	62.22	1.0333
NB	34.55	53.27	57.22	51.04	0.2667
LR	74.55	70.07	69.67	69.64	2.5133
GB	100.00	100.00	100.00	100.00	55.4777
SVC	94.33	80.86	80.33	80.19	1.0400
Adaboost	75.11	77.00	75.00	73.00	8.6900

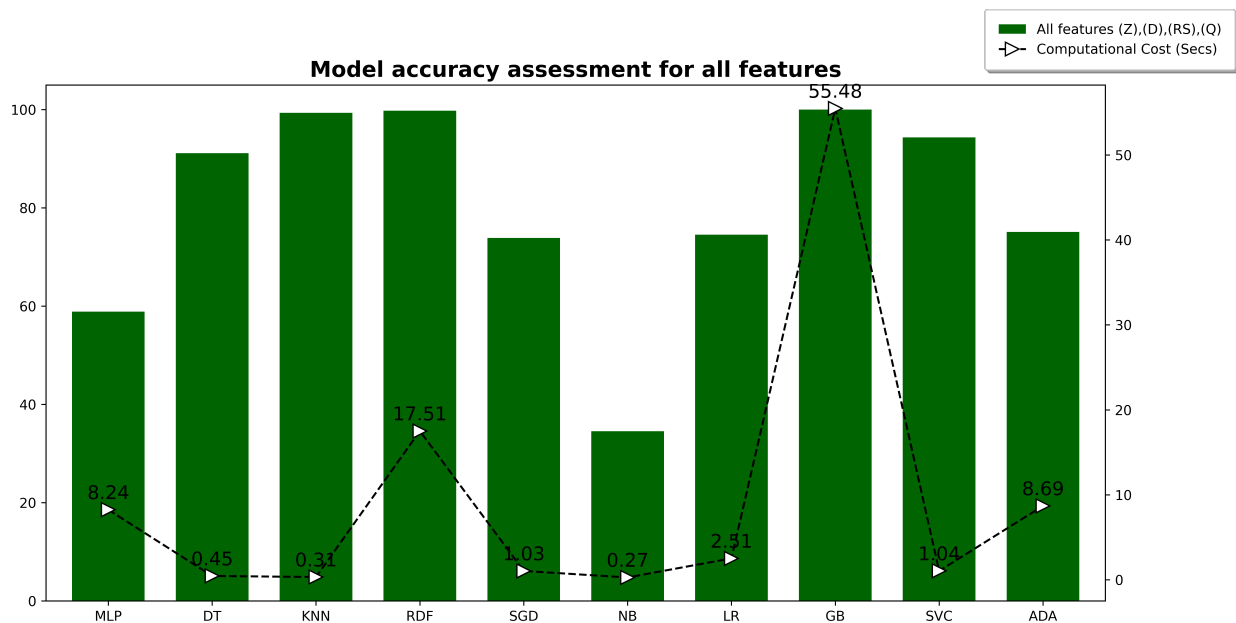


Figure 11. Model accuracy assessment for each all features (D-Q-RS-Z).

Interestingly, we explored the option of an individual and dual input parameter for the model to compare its performance with using total features. The Table 1 gives a better insight into the combination of the features for the model evaluation with the individual input parameter shown in Table 6—for the impedance, Table 7 for the loss

coefficient/dissipation factor, Table 8 for the equivalent series resistance and Table 9 for the quality factor. Figure 12 shows the bar plot of the model accuracy of the individual approach and also displays the average computational cost across the model for the individual features. The impedance (Z), loss coefficient (D), ESR, and quality factor (Q) are in blue, orange, green and red colours, respectively. In terms of accuracy and consistency, it can be seen that KNN and GBC rank top. In contrast, in terms of computational cost (s), the NB (0.233875), KNN (0.302475), DT (0.3758) and SVC (0.765) s in that order have the most negligible average value across the individual feature model performance evaluation. Interestingly, NB predicted poorly with an average accuracy of 73.885% across the input parameters. At the same time, KNN ranks the highest in terms of accuracy (98.19%) and the least computational cost, DT with an average accuracy (94.4125%) follows RDF with an average accuracy of 95.915% but with an average computational cost of 15.49399 s which shows it can not be considered for a cost-aware application.

Table 6. Global performance comparison of ML models using impedance (Z) features.

Algorithm	Accuracy (%)	Precision (%)	Recall (%)	F1-Score (%)	Cost (s)
MLP	48.77	46.49	48.78	43.53	7.6400
DT	91.44	92.37	91.56	91.55	0.3700
KNN	98.22	98.27	98.22	98.22	0.2833
RDF	91.78	91.94	91.78	91.72	15.8266
SGD	73.00	74.45	73.00	69.36	1.2266
NB	48.22	44.85	48.22	38.49	0.2200
LR	71.56	70.93	71.56	70.53	3.4933
GB	99.11	99.12	99.11	99.11	50.1100
SVC	89.78	90.53	89.78	89.28	1.2000
Adaboost	88.78	89.98	88.78	88.89	8.7733

Table 7. Global performance comparison of ML models using loss coefficient (D) features.

Algorithm	Accuracy (%)	Precision (%)	Recall (%)	F1-Score (%)	Cost (s)
MLP	86.88	88.83	86.89	86.82	9.1933
DT	90.11	90.88	91.66	88.89	0.4066
KNN	98.44	97.76	98.89	99.44	0.3067
RDF	95.44	98.67	97.22	98.22	15.6333
SGD	78.44	87.45	76.89	86.44	1.1222
NB	68.88	78.88	76.66	76.66	0.2267
LR	92.66	89.00	91.11	89.55	2.8867
GB	99.44	100.00	100.00	100.00	52.7111
SVC	93.33	96.66	96.66	96.66	0.7267
Adaboost	93.78	93.33	93.33	93.33	8.8133

Table 8. Global performance comparison of ML models using (ESR) features.

Algorithm	Accuracy (%)	Precision (%)	Recall (%)	F1-Score (%)	Cost (s)
MLP	93.33	93.28	93.25	93.41	10.2133
DT	98.33	98.33	98.35	98.36	0.3333
KNN	99.33	99.34	99.36	99.34	0.3066
RDF	99.33	99.36	99.33	99.32	15.3333
SGD	94.33	94.32	94.33	94.34	0.7733
NB	95.11	95.11	95.09	95.10	0.2444
LR	92.89	93.00	92.89	93.00	2.4888
GB	100.00	100.00	100.00	100.00	44.3967
SVC	98.33	98.32	98.34	98.33	0.5667
Adaboost	97.77	97.75	97.72	97.75	8.3333

Table 9. Global performance comparison of ML models using quality factor (Q) features.

Algorithm	Accuracy (%)	Precision (%)	Recall (%)	F1-Score (%)	Cost (s)
MLP	87.56	87.55	87.54	87.56	5.2133
DT	97.77	97.25	97.11	97.11	0.3933
KNN	99.66	99.67	99.67	99.67	0.3133
RDF	97.11	95.26	94.67	94.63	15.7267
SGD	89.77	89.35	87.89	87.72	0.9999
NB	83.33	83.00	74.11	69.93	0.2444
LR	89.22	89.43	89.33	89.32	2.2222
GB	99.55	99.46	99.44	99.44	54.8233
SVC	94.55	95.54	95.11	95.10	0.5666
Adaboost	81.88	84.00	82.00	81.00	9.0733

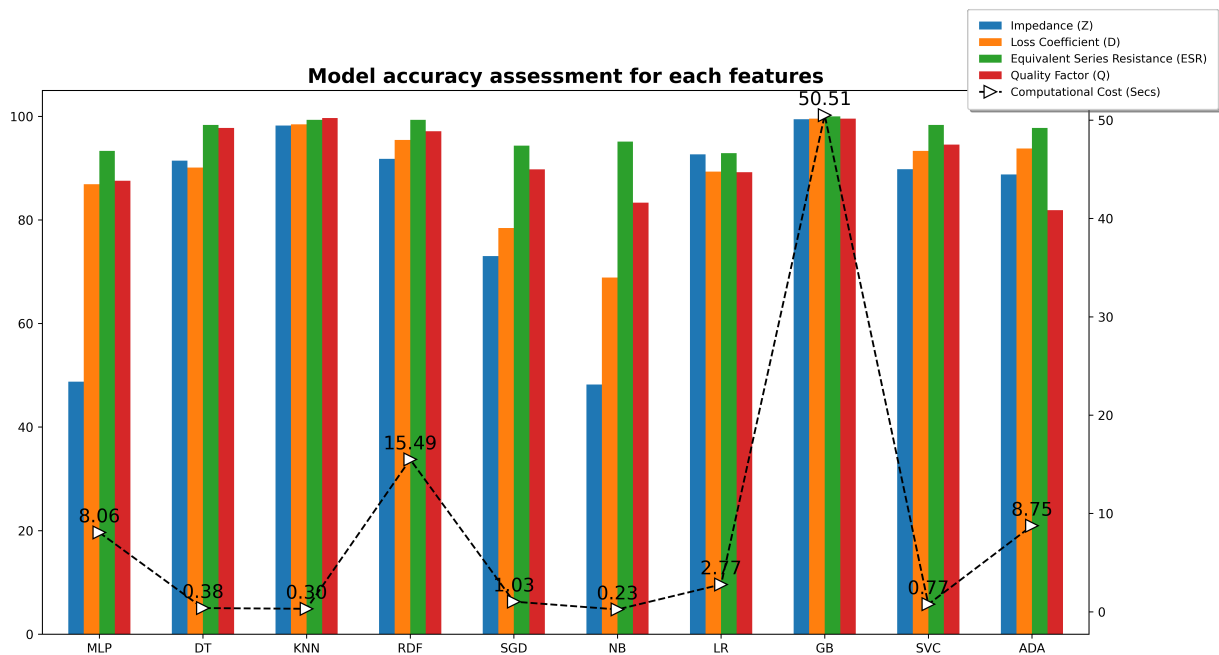


Figure 12. Model accuracy assessment for single features.

In terms of individual model performance and features, the ESR features showed a better prediction across all the models, further validating its importance as the best feature for diagnosing an aluminium electrolytic capacitors found in SMPS. The prediction for ESR stands out for all the models except for KNN and GB, which had a minimal difference in accuracy among the single features. Also, the quality factor (Q) ranks second as a more diagnostics tool in terms of performance across the models selected with loss coefficient (D) and impedance (Z) with the least performance accuracy of 89.419% and 82.209% respectively. Furthermore, we explored the option of combining two electrical parameters and checking for their performance on the models.

Tables 10–15 shows the dual feature set performance evaluation in the order, impedance + dissipation factor (ZD), ESR + quality factor (RSD), ESR + impedance (RSZ), quality factor + impedance (QZ), quality factor + dissipation factor (QD) and ESR + dissipation factor (RSD) respectively. Figure 13 shows the bar plot for all the dual feature sets with their average computational cost. KNN, RDF and GB ranked high in accuracy and consistency across all the dual feature sets as the models predicted accurately with an average computational cost of 0.287767, 15.6311, and 50.78665 s.

Table 10. Global performance comparison of ML models using combination of (Z) and (D) features.

Algorithm	Accuracy (%)	Precision (%)	Recall (%)	F1-Score (%)	Cost (s)
MLP	61.89	66.88	66.44	64.81	9.4444
DT	94.00	88.38	83.00	81.95	0.3444
KNN	99.44	98.62	98.56	98.56	0.2800
RDF	99.00	96.29	96.11	96.09	15.7533
SGD	74.44	87.57	85.00	84.33	1.1667
NB	57.22	63.00	50.11	45.28	0.2333
LR	69.55	68.34	69.44	67.69	3.0066
GB	99.88	99.78	99.78	99.78	50.8233
SVC	94.88	78.1	75.67	73.4	1.0800
Adaboost	99.22	88.45	83.89	82.94	8.8933

Table 11. Global performance comparison of ML models using combination of (RS) and (Q) features.

Algorithm	Accuracy (%)	Precision (%)	Recall (%)	F1-Score (%)	Cost (s)
MLP	71.22	73.01	71.22	67.94	8.4533
DT	96.67	96.69	96.33	96.34	0.4133
KNN	98.67	98.70	98.67	98.67	0.2933
RDF	99.22	95.85	95.44	95.48	15.5867
SGD	95.11	91.73	89.00	88.37	0.7933
NB	71.67	67.70	66.11	64.00	0.2133
LR	87.56	88.69	88.00	87.84	3.0933
GB	99.67	99.25	99.22	99.22	53.7633
SVC	97.11	94.48	94.11	94.08	0.6867
Adaboost	84.56	86.95	86.56	86.41	9.0067

Table 12. Global performance comparison of ML models using combination of (RS) and (Z) features.

Algorithm	Accuracy (%)	Precision (%)	Recall (%)	F1-Score (%)	Cost (s)
MLP	58.33	58.90	58.33	53.62	7.8444
DT	96.00	95.85	95.56	95.55	0.4267
KNN	98.00	98.05	98.00	98.00	0.2733
RDF	96.00	94.05	94.00	93.95	15.9200
SGD	96.00	95.84	95.44	95.43	0.8800
NB	60.00	65.93	58.56	56.20	0.2200
LR	62.45	63.34	62.22	60.87	3.1867
GB	99.32	99.45	99.11	99.22	57.9633
SVC	84.00	96.50	96.33	96.34	0.7933
Adaboost	96.32	96.78	96.11	96.04	8.1800

Table 13. Global performance comparison of ML models using combination of (Q) and (Z) features.

Algorithm	Accuracy (%)	Precision (%)	Recall (%)	F1-Score (%)	Cost (s)
MLP	75.88	77.02	75.89	75.64	10.1400
DT	84.33	89.08	84.11	83.43	0.3267
KNN	97.55	97.97	97.78	97.75	0.2800
RDF	98.44	96.85	96.78	96.76	15.3333
SGD	80.22	79.70	78.00	74.49	0.9067
NB	33.66	51.60	52.67	42.16	0.2067
LR	77.88	78.28	77.78	77.36	2.5067
GB	100.00	99.45	99.44	99.44	45.2500
SVC	79.88	79.57	78.00	77.01	0.7267
Adaboost	83.22	88.02	85.78	85.18	8.2467

Table 14. Global performance comparison of ML models using combination of (Q) and (D) features.

Algorithm	Accuracy (%)	Precision (%)	Recall (%)	F1-Score (%)	Cost (s)
MLP	44.22	38.68	44.22	32.79	5.8133
DT	83.88	89.01	85.56	84.66	0.4333
KNN	99.88	98.38	98.33	98.33	0.3000
RDF	96.88	97.03	96.89	96.88	15.6867
SGD	85.00	88.02	84.89	83.54	0.9533
NB	43.33	45.48	50.44	43.87	0.2200
LR	77.67	73.70	74.56	73.30	2.8733
GB	99.88	99.57	99.56	99.56	55.4167
SVC	89.11	87.55	86.78	86.7	0.8667
Adaboost	99.56	96.02	95.78	95.73	9.3333

Table 15. Global performance comparison of ML models using combination of (RS) and (D) features.

Algorithm	Accuracy (%)	Precision (%)	Recall (%)	F1-Score (%)	Cost (s)
MLP	29.67	24.33	29.67	24.46	4.7667
DT	92.88	91.94	90.00	89.80	0.3000
KNN	99.55	98.16	98.11	98.11	0.2600
RDF	95.78	94.69	94.44	94.45	15.5066
SGD	91.22	73.25	65.67	61.53	1.1933
NB	33.78	52.18	45.78	41.06	0.2333
LR	80.44	81.87	80.43	80.45	2.8333
GB	99.77	99.78	99.75	99.77	41.5033
SVC	92.00	91.28	91.45	91.67	1.3667
Adaboost	89.22	89.56	88.22	89.47	8.2133

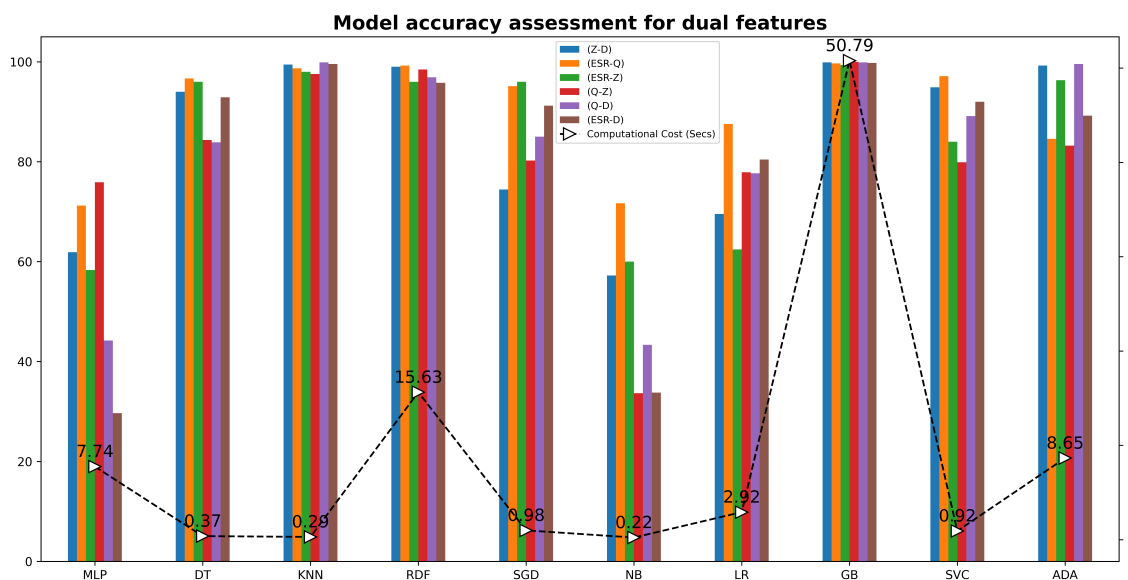


Figure 13. Model accuracy assessment for dual features.

Going by the individual model for the dual features performance comparison, the multi-perception (MLP)—a fully connected class of feed-forward artificial neural network has average accuracy and computational cost (56.8683% and 7.74368 s), respectively. The combination of ESR and Q stands out for the MLP in terms of accuracy and computational costs. With (RSQ) dual features with the highest accuracy. The decision tree (DT)—easy and intuitive with its tree-based classification rules has average accuracy and computational cost (91.2933% and 0.374067 s), respectively, with the (RSZ) dual feature with a better prediction. The k nearest neighbours (KNN)—a supervised learning algorithm that looks to

its surrounding data and classifies them, resulted in an average accuracy and computational cost (98.8483% and 0.287767 s). With a better discriminant performance using the (QD) dual feature with a 99.88% accuracy.

The random forest (RDF)—an ensemble learning classification with a collection of the decision tree has an average accuracy and computation cost (97.5533% and 15.6311 s), respectively. The stochastic gradient (SGD), Naive Bayes (NB), and logistic regression (LR) has an average accuracy and computational cost (86.9983%, 49.9433%, 75.9250% and 0.9822167, 0.2211, 2.91665 s). Noticeably, the NB model seems to have the least computational cost among the models but with a poor prediction for the dual feature. The gradient boost algorithm (GB)—with a primary idea to develop models sequentially, with each model attempting to reduce the mistakes of the previous model. The GB had consistent accuracy across all the dual features with average accuracy and computational cost (99.7533% and 50.78665 s). The support vector classifier (SVC)—a set of supervised learning models with practical advantages in high dimensional spaces has average accuracy and computational cost (89.4967% and 0.9200 s), respectively, with the (RSQ) dual feature ranking high among other features.

Furthermore, last but not least, the Adaboost model—an ensemble learning algorithm that uses an iterative mode to learn and combine weak classifier with building a more robust classifier with average accuracy and computational cost (92.0167% and 8.64555 s) across the dual features with the (QD) features ranking high among its peer. Finally, by assessing the results from the dual features, the ESR and Q have the highest occurrence, which shows they both have the needed discriminative features to act as a diagnostic tool either as a standalone feature or combination of features. The comparison among the feature selection has given insights into this methodology and can be replicated for other power electronic devices.

Figure 14 shows the fault visualization of the three output aluminium electrolytic capacitors using the principal component analysis (PCA). The label colour (blue, red and green) shows the 2200 uf, 1000 uf and 470 uf capacitors. The PCA has helped reduce the entire dataset (an initial seven feature selection) to a new set of features (two features). The approach assisted in giving an insight into the fault classification space of the capacitors.

Overall, the KNN model performance across all the feature selection method were outstanding in terms of accuracy and computational cost. Also, the ensemble method (RDF and GB) had good accuracy across the feature selection method but with a higher computational cost. With this few point, in terms of accuracy, the gradient boost model is the ideal model for application while in terms of computational cost, the KNN model is to be selected due to its simplicity. It has been able to outperform other classifier with this set of data from the aluminum electrolytic capacitors. To corroborate the model selection, the most performing feature (ESR) confusion matrix is shown in Figure 15 across the machine learning algorithm selected. The label (0,1,2) denotes the three capacitors respectively in order of their capacitance value (2200 uf, 100 uf, and 470 uf).

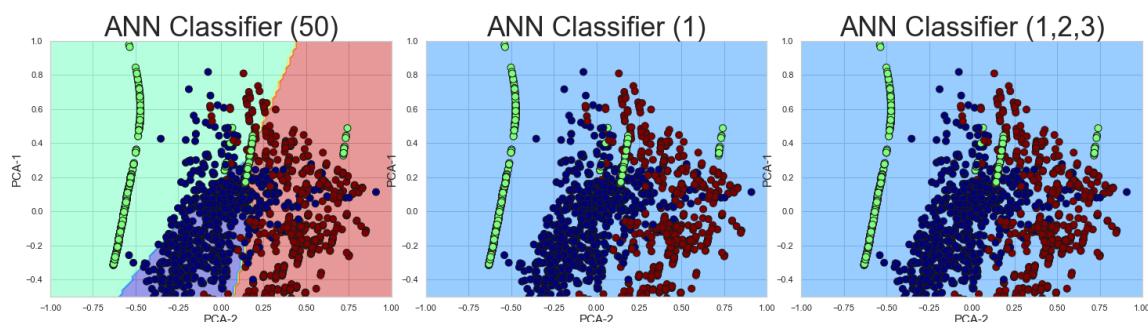


Figure 14. Fault Visualization Plot for the Aluminum Electrolytic Capacitors.

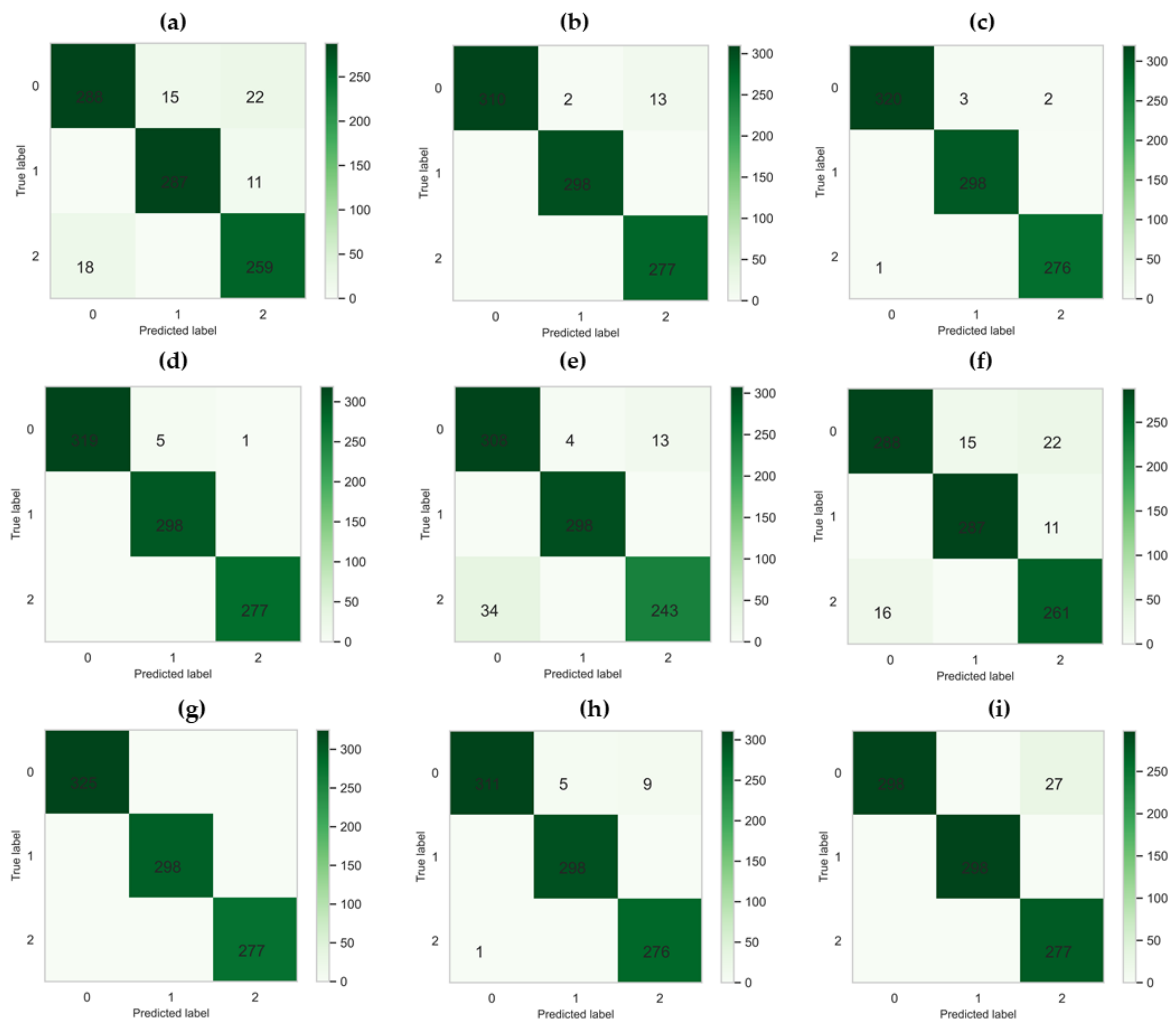


Figure 15. Confusion Matrix of the selected models (a) MLP (b) DT (c) KNN (d) RF (e) SGD (f) LR (g) GB (h) SVC (i) Adaboost

7. Conclusions and Future Works

The proposed approach provides an experimental architecture compared to the online method using ESR and C values estimation from voltage and current signals sampling. The proposed method (offline) directly acquires the selected electrical signals that can act as a health indicator for the aluminium electrolytic capacitors diagnosis. Also, the method proposed offers a more reliable and accurate condition monitoring that can be replicated easily in an industrial environment.

In this study, a multi parameter condition monitoring framework is proposed for fault diagnosis in output capacitors of SMPS. The aluminium electrolytic capacitors deterioration is characterized by different electrical parameters with the equivalent series resistance having the best discriminating features to classify the models. The input and output capacitance of any power system are critical to its overall performance. Different types of capacitors will be used in a well-designed power supply decoupling network and the amount and type of capacitors used in any design will be determined by the system design requirements. A reliable, low-cost power system can be created by following the capacitor recommendations in the data sheet and selecting capacitors depending on your actual operating conditions. With other various capacitor type available, aluminium electrolytic capacitors are mostly selected due to their superior energy density and cost effectiveness.

Interestingly, we have correlated a statistical feature engineering approach with various machine learning models on the electrical signals from the HIOKI 3536 LCR. The

major contribution of this study is the extraction and selection of a substantial features for improved offline condition monitoring techniques at the right computational costs. We have also adopted a wide range comparison among different classification algorithm to aid the decision making tool and deployment for practical applications.

The single feature approach has a better performance ratio compared to the dual and all feature approaches among the different feature selection techniques adopted. Also, the advantages of various parameters like data size, number of hyperparameters, missing values, outliers, and feature scaling paved way for improved performance among some of the models. This study has illustrated the effectiveness of the proposed condition monitoring method on aluminum electrolytic capacitor subjected to a similar charging and discharging cycle using the advanced HIOKI 3536 LCR meter.

This methodology can be replicated for most power electronics component like inductors, transistor etc by identifying the right parameters to be supervised for their condition monitoring process. For future studies, we would direct our aim to a temperature dependent condition monitoring using a filtering mechanism combined with deep learning models.

Author Contributions: Conceptualization A.B.K., methodology A.B.K.; software A.B.K. and J.-W.H.; validation A.B.K.; formal analysis A.B.K.; investigation A.B.K.; data curation A.B.K.; writing—original draft preparation A.B.K.; writing—review and editing A.B.K.; and visualization A.B.K.; resources and supervision J.-W.H.; project administration J.-W.H.; and funding acquisition J.-W.H. All authors have read and agreed to the published version of the manuscript.

Funding: This research was supported by the MSIT (Ministry of Science and ICT), Korea, under the Grand Information Technology Research Center support program (IITP-2020-2020-0-01612) supervised by the IITP (Institute for Information and communications Technology Planning and Evaluation).

Institutional Review Board Statement: Not applicable.

Informed Consent Statement: Not applicable.

Data Availability Statement: The data presented in this study are available on request from the corresponding author. The data are not publicly available due to laboratory regulations.

Conflicts of Interest: The authors declare no conflict of interest.

References

1. Kim, S.; Choi, J.-H.; Kim, N.H. Challenges and Opportunities of System-Level Prognostics. *Sensors* **2021**, *21*, 7655. [[CrossRef](#)] [[PubMed](#)]
2. Akpudo, U.E.; Hur, J.-W. Investigating the Efficiencies of Fusion Algorithms for Accurate Equipment Monitoring and Prognostics. *Energies* **2022**, *15*, 2204. [[CrossRef](#)]
3. Cofre-Martel, S.; Lopez Droguett, E.; Modarres, M. Big Machinery Data Preprocessing Methodology for Data-Driven Models in Prognostics and Health Management. *Sensors* **2021**, *21*, 6841. [[CrossRef](#)] [[PubMed](#)]
4. Falck, J.; Felgemacher, C.; Rojko, A.; Liserre, M.; Zacharias, P. Reliability of Power Electronic Systems: An Industry Perspective. *IEEE Ind. Electron. Mag.* **2018**, *12*, 24–35. [[CrossRef](#)]
5. Zhang, P.; Gao, Z.; Cao, L.; Dong, F.; Zou, Y.; Wang, K.; Zhang, Y.; Sun, P. Marine Systems and Equipment Prognostics and Health Management: A Systematic Review from Health Condition Monitoring to Maintenance Strategy. *Machines* **2022**, *10*, 72. [[CrossRef](#)]
6. Pellitteri, F.; Di Dio, V.; Puccio, C.; Miceli, R. A Model of DC-DC Converter with Switched-Capacitor Structure for Electric Vehicle Applications. *Energies* **2022**, *15*, 1224. [[CrossRef](#)]
7. Omid, H.; Yaser, D. Reliability modelling of capacitor voltage transformer using proposed Markov model. *Electric Power Syst. Res.* **2022**, *202*, 107573. ISSN 0378-7796. [[CrossRef](#)]
8. Summer, F.; Torop, J.; Aabloo, A.; Kyritsakis, A.; Zadin, V. Particle Dynamics-Based Stochastic Modeling of Carbon Particle Charging in the Flow Capacitor Systems. *Appl. Sci.* **2022**, *12*, 1887. [[CrossRef](#)]
9. Bi, K. A Model Predictive Controlled Bidirectional Four Quadrant Flying Capacitor DC/DC Converter Applied in Energy Storage System. *IEEE Trans. Power Electron.* **2022**, *37*, 7705–7717. [[CrossRef](#)]
10. Mcgrew, T.; Sysoeva, C.V.; Cheng, H.; Miller, C.; Scofield, J.; Scott, M.J. Condition Monitoring of DC-Link Capacitors using Time-Frequency Analysis and Machine Learning Classification of Conducted EMI. *IEEE Trans. Power Electron.* **2022**. [[CrossRef](#)]
11. Zhang, Y.; Yao, C.; Gao, F.; Song, T.; Tang, Y.; Zhu, X. Motor Driver-Based Topology of Integrated On-Board Charging System and Data-Driven Inductance Identification Method. *IEEE J. Emerg. Sel. Top. Circuits Syst.* **2022**, *12*, 310–319. [[CrossRef](#)]
12. Chen, J.; Zhao, Y.; Xue, X.; Chen, R.; Wu, Y. Data-Driven Health Assessment in a Flight Control System under Uncertain Conditions. *Appl. Sci.* **2021**, *11*, 10107. [[CrossRef](#)]

13. Shifat, T.A.; Yasmin, R.; Hur, J.-W. A Data Driven RUL Estimation Framework of Electric Motor Using Deep Electrical Feature Learning from Current Harmonics and Apparent Power. *Energies* **2021**, *14*, 3156. [[CrossRef](#)]
14. Bhargava, C. Review of Health Prognostics and Condition Monitoring of Electronic Components. *IEEE Access* **2020**, *8*, 75163–75183. [[CrossRef](#)]
15. Zhao, S.; Makis, V.; Chen, S.; Li, Y. Health Assessment Method for Electronic Components Subject to Condition Monitoring and Hard Failure. *IEEE Trans. Instrum. Meas.* **2019**, *68*, 138–150. [[CrossRef](#)]
16. Kim, S.; Akpudo, U.E.; Hur, J.-W. A Cost-Aware DNN-Based FDI Technology for Solenoid Pumps. *Electronics* **2021**, *10*, 2323. [[CrossRef](#)]
17. Lee, M.-S.; Shifat, T.A.; Hur, J.W. Kalman Filter Assisted Deep Feature Learning for RUL Prediction of Hydraulic Gear Pump. *IEEE Sens. J.* **2022**. [[CrossRef](#)]
18. Shifat, T.A.; Hur, J.W. ANN Assisted Multi Sensor Information Fusion for BLDC Motor Fault Diagnosis. *IEEE Access* **2021**, *9*, 429–9441. [[CrossRef](#)]
19. Narale S. B.; Verma A.; and Anand S. Accelerated Aging Method and Lifetime Evaluation of Aluminum Electrolytic Capacitors for Power Electronic Application. In Proceedings of the 2020 IEEE Energy Conversion Congress and Exposition (ECCE), Detroit, MI, USA, 11–15 October 2020; pp. 3662–3669. [[CrossRef](#)]
20. Ren, L.; Zhang, L.; Gong, C. ESR Estimation Schemes of Output Capacitor for Buck Converter from Capacitor Perspective. *Electronics* **2020**, *9*, 1596. [[CrossRef](#)]
21. Amaral, A.M.R.; Cardoso, A.J.M. A Simple Offline Technique for Evaluating the Condition of Aluminum–Electrolytic–Capacitors. *IEEE Trans. Ind. Electron.* **2009**, *56*, 3230–3237. [[CrossRef](#)]
22. Amaral, A.M.R.; Cardoso, A.J.M. An Economic Offline Technique for Estimating the Equivalent Circuit of Aluminum Electrolytic Capacitors. *IEEE Trans. Instrum. Meas.* **2008**, *57*, 2697–2710. [[CrossRef](#)]
23. Rojas-Dueñas, G.; Riba, J.-R.; Moreno-Eguilaz, M. CNN-LSTM-Based Prognostics of Bidirectional Converters for Electric Vehicles' Machine. *Sensors* **2021**, *21*, 7079. [[CrossRef](#)] [[PubMed](#)]
24. Pu, X.; Nguyen, T.H.; Lee, D.; Lee, K.; Kim, J. Fault Diagnosis of DC-Link Capacitors in Three-Phase AC/DC PWM Converters by Online Estimation of Equivalent Series Resistance. *IEEE Trans. Ind. Electron.* **2013**, *60*, 4118–4127. [[CrossRef](#)]
25. Miao, W.; Liu, X.; Lam, K.H.; Pong, P.W.T. Condition Monitoring of Electrolytic Capacitors in Boost Converters by Magnetic Sensors. *IEEE Sens. J.* **2019**, *19*, 10393–10402. [[CrossRef](#)]
26. Laadjal, K.; Sahraoui, M.; Cardoso, A.J.M. On-Line Fault Diagnosis of DC-Link Electrolytic Capacitors in Boost Converters Using the STFT Technique. *IEEE Trans. Power Electron.* **2021**, *36*, 6303–6312. [[CrossRef](#)]
27. Ghadrhan, M.; Peyghami, S.; Mokhtari, H.; Blaabjerg, F.O.G. Condition Monitoring of DC-link Electrolytic Capacitor in Back-to-Back Converters Based on Dissipation Factor. *IEEE Trans. Power Electron.* **2022**, *37*, 733–9744. [[CrossRef](#)]
28. Xin, X.; Yang, Y.; Ma, K.; He, B. Online Monitoring for Sub-module Capacitance in Modular Multilevel Converter with Four Sampling Points of Capacitor Voltage. In Proceedings of the 2020 IEEE 9th International Power Electronics and Motion Control Conference (IPEMC2020-ECCE Asia), Nanjing, China, 29 November–2 December 2020; pp. 935–939. [[CrossRef](#)]
29. Rodriguez Ramos, E.; Leyva, R.; Farivar, G.G.; Townsend, C.D.; Pou, J. Capacitor Condition Monitoring for the Low-Capacitance StatCom: An Online Approach. *IEEE Trans. Power Electron.* **2022**, *37*, 3697–3701. [[CrossRef](#)]
30. Asoodar, M.; Nahalparvari, M.; Danielsson, C.; Söderström, R.; Nee, H.P. Online Health Monitoring of DC-Link Capacitors in Modular Multilevel Converters for FACTS and HVDC Applications. *IEEE Trans. Power Electron.* **2021**, *36*, 13489–13503. [[CrossRef](#)]
31. Ren, L.; Gong, C.; Zhao, Y. An Online ESR Estimation Method for Output Capacitor of Boost Converter. *IEEE Trans. Power Electron.* **2019**, *34*, 10153–10165. [[CrossRef](#)]
32. Laadjal, K.; Bento, F.; Cardoso, A.J.M. On-Line Diagnostics of Electrolytic Capacitors in Fault-Tolerant LED Lighting Systems. *Electronics* **2022**, *11*, 1444. [[CrossRef](#)]
33. Zhao, Z.; Davari, P.; Lu, W.; Blaabjerg, F. Online DC-Link Capacitance Monitoring for Digital-Controlled Boost PFC Converters without Additional Sampling Devices. *IEEE Trans. Ind. Electron.* **2022**. [[CrossRef](#)]
34. Ghadrhan, M.; Abdi, B.; Peyghami, S.; Mokhtari, H.; Blaabjerg, F. On-line Condition Monitoring System for DC-link Capacitor of Back-to-Back Converters Using Large-signal Transients. *IEEE J. Emerg. Sel. Top. Power Electron.* **2022**. [[CrossRef](#)]
35. Wang, F.; Cai, Y.; Tang, H. Prognostics of Aluminum Electrolytic Capacitors Based on Chained-SVR and 1D-CNN Ensemble Learning. *Arab. J. Sci. Eng.* **2022**. [[CrossRef](#)]
36. Harada, K.; Katsuki, A.; Fujiwara, M. Use of ESR for deterioration diagnosis of electrolytic capacitor. *IEEE Trans. Power Electron.* **1993**, *8*, 355–361. [[CrossRef](#)]
37. Hao, M.; Wang, L. Fault diagnosis and failure prediction of aluminum electrolytic capacitors in power electronic converters. In Proceedings of the 31st Annual Conference of IEEE Industrial Electronics Society, Raleigh, NC, USA, 6–10 November 2005; p. 6. [[CrossRef](#)]
38. Rigamonti, M.; Baraldi, P.; Zio, E.; Astigarraga, D.; Galarza, A. Particle Filter-Based Prognostics for an Electrolytic Capacitor Working in Variable Operating Conditions. *IEEE Trans. Power Electron.* **2016**, *31*, 1567–1575. [[CrossRef](#)]
39. Kulkarni, C.S.; Celaya, J.R.; Goebel, K.; Biswas, G. Physics Based Electrolytic Capacitor Degradation Models for Prognostic Studies under Thermal Overstress. *PHM Soc. Eur. Conf.* **2012**, *1*. [[CrossRef](#)]

40. Celaya, J.R.; Kulkarni, C.; Saha, S.; Biswas, G.; Goebel, K. Accelerated aging in electrolytic capacitors for prognostics. In Proceedings of the 2012 Proceedings Annual Reliability and Maintainability Symposium, Reno, NV, USA, 23–26 January 2012; pp. 1–6. [CrossRef]
41. Kulkarni, C.; Biswas, G.; Koutsoukos, X.; Celaya, J.; Goebel, K. Integrated diagnostic/prognostic experimental setup for capacitor degradation and health monitoring. In Proceedings of the 2010 IEEE Autotestcon, Orlando, FL, USA, 13–16 September 2010; pp. 1–7. [CrossRef]
42. Kareem, A.B.; Ejike Akpudo, U.; Hur, J.-W. An Integrated Cost-Aware Dual Monitoring Framework for SMPS Switching Device Diagnosis. *Electronics* **2021**, *10*, 2487. [CrossRef]
43. García, E.M.; Alberti, M.G.; Arcos Álvarez, A.A. Measurement-While-Drilling Based Estimation of Dynamic Penetrometer Values Using Decision Trees and Random Forests. *Appl. Sci.* **2022**, *12*, 4565. [CrossRef]
44. Li, Q.; Zhao, C.; He, X.; Chen, K.; Wang, R. The Impact of Partial Balance of Imbalanced Dataset on Classification Performance. *Electronics* **2022**, *11*, 1322. [CrossRef]
45. Talebi, S.; Waczak, J.; Fernando, B.A.; Sridhar, A.; Lary, D.J. Data-Driven EEG Band Discovery with Decision Trees. *Sensors* **2022**, *22*, 3048. [CrossRef]
46. Lee, S.-J.; Tseng, C.-H.; Yang, H.-Y.; Jin, X.; Jiang, Q.; Pu, B.; Hu, W.-H.; Liu, D.-R.; Huang, Y.; Zhao, N. Random RotBoost: An Ensemble Classification Method Based on Rotation Forest and AdaBoost in Random Subsets and Its Application to Clinical Decision Support. *Entropy* **2022**, *24*, 617. [CrossRef]
47. Huang, J.; Ling, S.; Wu, X.; Deng, R. GIS-Based Comparative Study of the Bayesian Network, Decision Table, Radial Basis Function Network and Stochastic Gradient Descent for the Spatial Prediction of Landslide Susceptibility. *Land* **2022**, *11*, 436. [CrossRef]
48. Masood, H.; Zafar, A.; Ali, M.U.; Hussain, T.; Khan, M.A.; Tariq, U.; Damaševičius, R. Tracking of a Fixed-Shape Moving Object Based on the Gradient Descent Method. *Sensors* **2022**, *22*, 1098. [CrossRef]
49. Franzese, G.; Milios, D.; Filippone, M.; Michiardi, P. A Scalable Bayesian Sampling Method Based on Stochastic Gradient Descent Isotropization. *Entropy* **2021**, *23*, 1426. [CrossRef] [PubMed]
50. Kim, D.; Heo, T.-Y. Anomaly Detection with Feature Extraction Based on Machine Learning Using Hydraulic System IoT Sensor Data. *Sensors* **2022**, *22*, 2479. [CrossRef] [PubMed]
51. Zou, Y.; Gao, C. Extreme Learning Machine Enhanced Gradient Boosting for Credit Scoring. *Algorithms* **2022**, *15*, 149. [CrossRef]
52. Kim, C.; Park, T. Predicting Determinants of Lifelong Learning Intention Using Gradient Boosting Machine (GBM) with Grid Search. *Sustainability* **2022**, *14*, 5256. [CrossRef]
53. Zheng, H.; Xiao, F.; Sun, S.; Qin, Y. Brillouin Frequency Shift Extraction Based on AdaBoost Algorithm. *Sensors* **2022**, *22*, 3354. [CrossRef]
54. Shifat, T.A.; Hur, J.W. Reliability improvement in the presence of weak fault features using non-Gaussian IMF selection and AdaBoost technique. *J. Mech. Sci. Technol.* **2021**, *35*, 3355–3367. [CrossRef]
55. Zou, X.; Wang, C.; Luo, M.; Ren, Q.; Liu, Y.; Zhang, S.; Bai, Y.; Meng, J.; Zhang, W.; Su, S.W. Design of Electronic Nose Detection System for Apple Quality Grading Based on Computational Fluid Dynamics Simulation and K-Nearest Neighbor Support Vector Machine. *Sensors* **2022**, *22*, 2997. [CrossRef]
56. Leon-Medina, J.X.; Anaya, M.; Pozo, F.; Tibaduiza, D. Nonlinear Feature Extraction Through Manifold Learning in an Electronic Tongue Classification Task. *Sensors* **2020**, *20*, 4834. [CrossRef] [PubMed]
57. Bhushan, S.; Alshehri, M.; Keshta, I.; Chakraverti, A.K.; Rajpurohit, J.; Abugabah, A. An Experimental Analysis of Various Machine Learning Algorithms for Hand Gesture Recognition. *Electronics* **2022**, *11*, 968. [CrossRef]
58. Peppes, N.; Daskalakis, E.; Alexakis, T.; Adamopoulou, E.; Demestichas, K. Performance of Machine Learning-Based Multi-Model Voting Ensemble Methods for Network Threat Detection in Agriculture 4.0. *Sensors* **2021**, *21*, 7475. [CrossRef]
59. Akpudo, U.E.; Jang-Wook, H. A Multi-Domain Diagnostics Approach for Solenoid Pumps Based on Discriminative Features. *IEEE Access* **2020**, *8*, 175020–175034. [CrossRef]
60. Current Dependency and Voltage Dependency | FAQ | Hioki. Available online: https://www.hioki.com/us-en/support/faq/detail/id_114 (accessed on 10 February 2022).
61. Contents. Available online: https://www.testequipmentdepot.com/hioki/pdf/bt3564_manual.pdf (accessed on 15 February 2022).
62. Kim, J.H.; Yoon, H.K.; Cho, S.; Kim, Y.; Lee, J. Four Electrode Resistivity Probe for Porosity Evaluation. *Geotech. Test. J.* **2011**, *34*. [CrossRef]
63. Satish, B.; Bharat K.; Sachin K.; Saxena A.K. Evaluation of four-terminal-pair capacitance standards using electrical equivalent circuit model, *Measurement* **2015**, *73*, 121–126. [CrossRef]
64. Hai, M.; Zhang, Y.; Yuejin, Z. A Performance Evaluation of Classification Algorithms for Big Data. *Procedia Comput. Sci.* **2017**, *122*, 1100–1107. [CrossRef]
65. Wong, T.T. Performance evaluation of classification algorithms by k-fold and leave-one-out cross validation. *Pattern Recognit.* **2015**, *48*, 2839–2846. [CrossRef]